Supporting Information for

Mechanistic insights into PFOS and PFOA adsorption on acid-resistant $MgTiO_3$

Seulgee Lee [a,†], *Fumitaka Hayashi* [a,b], *Kunio Yubuta* [a], *Eugenio Otal* [a], *Nagahiro Saito* [c,d,e], *Hideki Tanaka* [a], *Katsuya Teshima* [a,b,*]

[a] Institute for Aqua Regeneration, Shinshu University, 4-17-1 Wakasato, Nagano 380-8553, Japan

[b] Department of Materials Chemistry, Faculty of Engineering, Shinshu University, 4-17-1 Wakasato, Nagano 380-8553, Japan

[c] Department of Chemical Systems Engineering, Graduate School of Engineering, Nagoya University, Nagoya 464-8603, Japan

[d] Institute of Innovation for Future Society, Nagoya University, Nagoya 464-8603, Japan

[e] Conjoint Research Laboratory in Nagoya University, Shinshu University, Nagoya 464-8603, Japan

† Present address: Institute of Innovation for Future Society, Nagoya University, Nagoya 464-8603, Japan

*Corresponding author, E-mail: teshima@shinshu-u.ac.jp

Sections

1. Kinetic Models

Three complementary kinetic models were employed to analyze the time-dependent adsorption behavior and to elucidate the underlying rate-limiting mechanisms. First, the square-root-of-time linearization model, originally proposed by Weber and Morris for porous adsorbents,[1] was adapted for non-porous $MgTiO_3$ to diagnose diffusion-related mass-transfer processes. For this non-porous material, the Weber–Morris model reflects diffusion-related mass-transfer processes and is more appropriately interpreted in terms of boundary-layer diffusion. The model is expressed as:

$$q_t = k_d t^{1/2} + C \quad \text{(S1)}$$

, where q_t (mg g^{-1}) is the adsorbed amount at time t, k_d (mg g^{-1} $min^{1/2}$) is the diffusion rate parameter representing combined boundary layer and surface diffusion resistance, C (mg g^{-1}) is the intercept associated with boundary layer thickness and rapid initial adsorption, and t (min) is time. The square-root-of-time dependence originates from Fick's second law applied to semi-infinite diffusion layers, making this model diagnostic of diffusion-related mass-transfer behavior. Linear regressions of q_t versus $t^{1/2}$ were performed separately for each kinetic stage to extract k_d and C.

Second, the pseudo-second-order (PSO) kinetic model was applied using its linearized form:[2]

$$t/q_t = 1/(k_2 q_e^2) + t/q_e \quad \text{(S2)}$$

, where q_e (mg g^{-1}) is the equilibrium adsorption capacity, k_2 (g mg^{-1} min^{-1}) is the pseudo-second-order rate constant, and t (min) is time. Although the PSO model is often associated with chemisorption, it can also empirically describe diffusion-controlled processes. Here, it was used to quantify apparent rate constants and stage-specific adsorption capacities. Linear regression of t/q_t versus t yields q_e = 1/slope and k_2 = slope^2/intercept. The initial adsorption rate h_0 (mg g^{-1} min^{-1}) was calculated as $h_0 = k_2 q_e^2$.

Third, a double exponential model[3] was employed to deconvolute fast and slow processes without presupposing a transition time:

$$q_t = q_1(1 - e^{-k_1 t}) + q_2(1 - e^{-k_2 t}) \quad \text{(S3)}$$

, where q_1 and q_2 (mg g^{-1}) are the adsorption capacities associated with fast and slow processes, and k_1 and k_2 (min^{-1}) are the corresponding first-order rate constants. Non-linear regression was performed using the Levenberg-Marquardt algorithm, with initial parameter estimates obtained from preliminary data analysis. The half-life (min) for each process was calculated as $t_{1/2} = \ln(2)/k_{1,2}$, and the relative contribution of each process (%) was determined as:

$$\text{Contribution of process } i = [q_i/(q_1 + q_2)] \times 100\% \quad \text{(S4)}$$

For all kinetic models, the coefficient of determination (R^2) was calculated to evaluate the goodness of fit:

$$R^2 = 1 - (SS_{res}/SS_{tot}) \quad \text{(S5)}$$

, where $SS_{res} = \Sigma(y_{i,obs} - y_{i,pred})^2$ is the residual sum of squares and $SS_{tot} = \Sigma(y_{i,obs} - y_{mean})^2$ is the total sum of squares.

2. Adsorption Isotherm Models

Four adsorption isotherm models were applied to analyze the equilibrium adsorption data and to elucidate the possible adsorption mechanism.

First, the single-site Langmuir model, which assumes monolayer adsorption on energetically uniform sites, is expressed as:[4]

$$q_e = (q_{max}K_LC_e)/(1 + K_LC_e) \quad \text{(S6)}$$

, where q_e (mg g^{-1}) is equilibrium adsorption capacity, C_e (mg L^{-1}) is equilibrium concentration, q_{max} is maximum adsorption capacity (mg g^{-1}), and K_L (L mg^{-1}) is the Langmuir affinity constant. The dimensionless separation factor R_L, which indicates adsorption favorability, was calculated as:

$$R_L = 1/(1 + K_LC_0) \quad \text{(S7)}$$

, where C_0 (mg L^{-1}) is the initial concentration of solution.

Second, the two-site Langmuir model was employed to account for surface heterogeneity by considering two distinct types of adsorption sites:

$$q_e = (q_{max,1}K_{L1}C_e)/(1 + K_{L1}C_e) + (q_{max,2}K_{L2}C_e)/(1 + K_{L2}C_e) \quad \text{(S8)}$$

, where subscripts 1 and 2 denote high-affinity and low-affinity sites, respectively. The contribution of each site (%) was calculated as:

$$\text{Contribution of site } i = [q_{max,i}/(q_{max,1} + q_{max,2})] \times 100\% \quad \text{(S9)}$$

, and the affinity contrast between the two sites was quantified using the ratio K_{L1}/K_{L2}.

Third, the Freundlich model, which describes multilayer adsorption on heterogeneous surfaces, is given by:[5]

$$q_e = K_F\ C_e^{1/n} \quad \text{(S10)}$$

, where K_F ((mg g^{-1})·(L mg^{-1})$^{1/n}$) is the Freundlich capacity constant and n is the heterogeneity factor (dimensionless). Values of $n > 1$ indicate favorable adsorption.

Finally, the Sips (Langmuir-Freundlich combination) model combines features of both Langmuir and Freundlich isotherms and is express as:[6, 7]

$$q_e = (q_{max}K_S C_e^{n_s})/(1 + K_S C_e^{n_s}) \quad \text{(S11)}$$

, where K_S [(L mg^{-1})^{n_s}] is the Sips equilibrium constant and n_s is the heterogeneity parameter (dimensionless). When $n_s = 1$, the Sips model reduces to the Langmuir equation, whereas $n_s \neq 1$ reflects surface heterogeneity.

All isotherm models were fitted using nonlinear regression with the Levenberg–Marquardt algorithm. Initial parameter estimates were obtained from linearized forms of the models, where applicable, or from graphical inspection of the experimental data.

Table S1. Physicochemical properties of PFOA and PFOS.

Compound	Acronym	Structure	Chemical Formula	Molar mass (g/mol)	pK_a
Perfluorooctanoic acid	PFOA	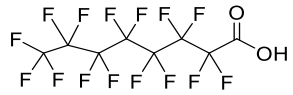	$C_8HF_{15}O_2$	414.07	−0.2[8]
Perfluorooctanesulfonic acid	PFOS	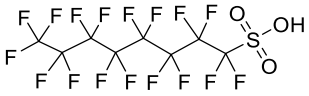	$C_8HF_{17}O_3S$	500.13	−3.27[9]

Table S2. Elemental composition (at.%) of MTO particles determined by EDS point analysis at regions 1 and 2 in **Figure S1**.

Point	O	Mg	Ti
1	65.25	19.81	14.94
2	68.59	16.63	14.79

Table S3. Kinetic parameters for PFOS and PFOA adsorption on $MgTiO_3$ (MTO).

Kinetic model	Parameter	PFOS adsorption	PFOA adsorption
Weber-Morris model (square-root-of-time linearization)	$k_{d,1}$	1.39×10^{-2}	6.56×10^{-3}
	$k_{d,2}$	1.92×10^{-3}	1.42×10^{-3}
	R_1^2	0.823	0.996
	R_2^2	0.952	0.966
	k_d ratio	7.250	4.603
PSO (pseudo-second-order)	$q_{e,1}$	0.368	0.123
	$q_{e,2}$	0.418	0.146
	$k_{2,1}$	7.36×10^{-2}	1.08×10^{-1}
	$k_{2,2}$	1.77×10^{-2}	5.90×10^{-3}
	$k_{2,1}/k_{2,2}$	4.16	18.28
	R_1^2	0.994	0.965
	R_2^2	0.927	1.000
	q_e_increase_%	13.5	18.7
DE (double exponential)	q_1	0.315	0.123
	q_2	0.095	0.137
	k_1	1.11×10^{-1}	6.56×10^{-2}
	k_2	1.80×10^{-3}	2.10×10^{-3}
	contrib_1_%	76.92	47.29
	contrib_2_%	23.08	52.71
	R^2	0.9615	0.9917

*Parameter units are defined in **Section 1**.

Table S4. Non-linear adsorption isotherm fitting parameters for PFOS and PFOA adsorption on MTO.

Adsorbate	Isotherm model	Parameter	Values	Adsorbate	Isotherm model	Parameter	Values
PFOS	Langmuir single-site	q_{max}	8.921	PFOA	Langmuir single-site	q_{max}	6.415
		K_L	0.301			K_L	0.104
		R^2	0.9878			R^2	0.9987
	Langmuir two-site	$q_{max,1}$	2.067		Langmuir two-site	$q_{max,1}$	1.316
		K_{L1}	2.199			K_{L1}	0.104
		$q_{max,2}$	9.507			$q_{max,2}$	5.100
		K_{L2}	9.8×10^{-2}			K_{L2}	0.104
		R^2	0.9953			R^2	0.9987
	Freundlich	K_F	2.1873		Freundlich	K_F	0.7712
		n	2.0841			n	1.6430
		R^2	0.9897			R^2	0.9919
	Sips	q_{max}	14.083		Sips	q_{max}	5.8339
		K_S	0.1861			K_S	0.1071
		n_s	0.6839			n_s	1.0829
		R^2	0.9947			R^2	0.9988

*Parameter units are defined in **Section 2**.

Table S5. Comparative Summary of PFOS and PFOA Adsorption Mechanisms on $MgTiO_3$.

Parameter	PFOS	PFOA
Mechanism	Single outer-sphere	Sequential dual (inner → outer)
Rate control	Diffusion (>95%)	Stage 1: Mixed (70-80% diffusion), Stage 2: Diffusion (>90%)
$k_{d,1}$ (mg g^{-1} $min^{-0.5}$)	1.39×10^{-2}	6.56×10^{-3}
$k_{d,2}$ (mg g^{-1} $min^{-0.5}$)	1.92×10^{-3}	1.42×10^{-3}
k_d ratio	7.25	4.60
$k_{2,1}$ (g mg^{-1} min^{-1})	7.36×10^{-2}	1.08×10^{-1}
$k_{2,2}$ (g mg^{-1} min^{-1})	1.77×10^{-2}	5.90×10^{-3}
k_2 ratio	4.16	18.28
k_1 (min^{-1})	1.11×10^{-1}	6.56×10^{-2}
k_2 (min^{-1})	1.80×10^{-3}	2.10×10^{-3}
k ratio	62.1	31.2
Fast contribution (%)	76.9	47.3
Slow contribution (%)	23.1	52.7
Capacity increase (%)	13.5	18.7
Stage 2 R^2 (PSO)	0.927	1.000
Transition time (min)	120	300
q_t at 960 min (mg g^{-1})	0.409 ± 0.001	0.260 ± 0.006
q_{max} equilibrium (mg g^{-1})	8.92	6.42
K_L (L mg^{-1})	0.301	0.104
FTIR $\Delta\nu$ (cm^{-1})	Outer-sphere only	246 (Inner-sphere)
Mechanism transition	No	Yes (120-300 min)

Table S6. ICP-OES analysis of Mg and Ti leaching (ppm) from MTO after PFAS adsorption at different pH levels.

Run	Sample	pH	Mg	Ti
1	MTO_PFOS	1.0	0.306	0.428
2	MTO_PFOA	1.0	0.285	0.328
3	MTO_PFOS	3.5	0.194	0.009
4	MTO_PFOA	3.5	0.155	0.009
5	MTO_PFOS	4.5	0.165	0.009
6	MTO_PFOA	4.5	0.112	0.008
7	MTO_PFOS	6.5	0.093	0.008
8	MTO_PFOA	6.5	0.136	0.009

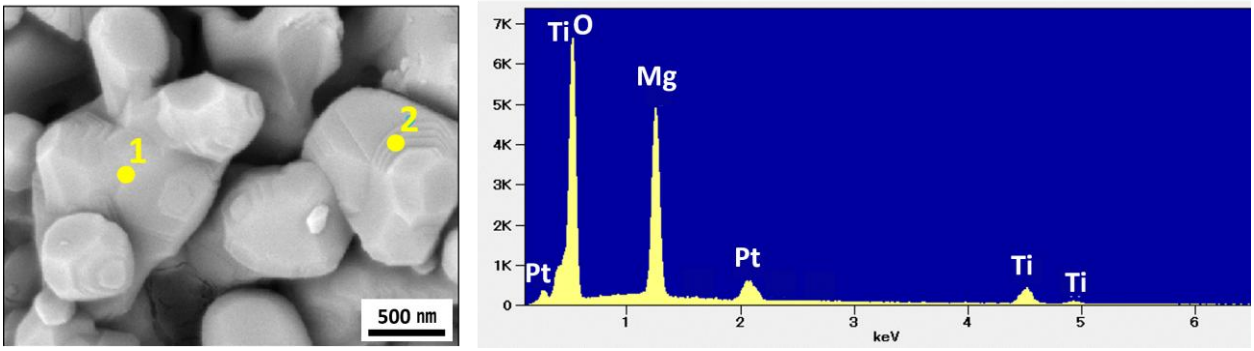

Figure S1. FE-SEM image and EDS spectrum of MTO particles. SEM was performed at an accelerating voltage of 7 kV after Pt coating. Yellow points (1, 2) indicate the regions selected for EDS point analysis.

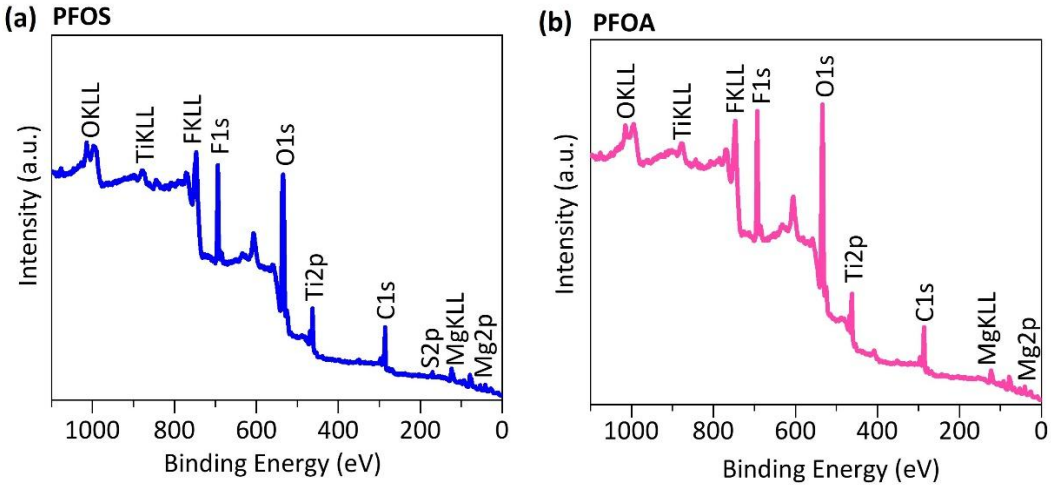

Figure S2. X-ray photoelectron spectroscopy (XPS) survey spectra of MTO after adsorption of (a) PFOS and (b) PFOA.

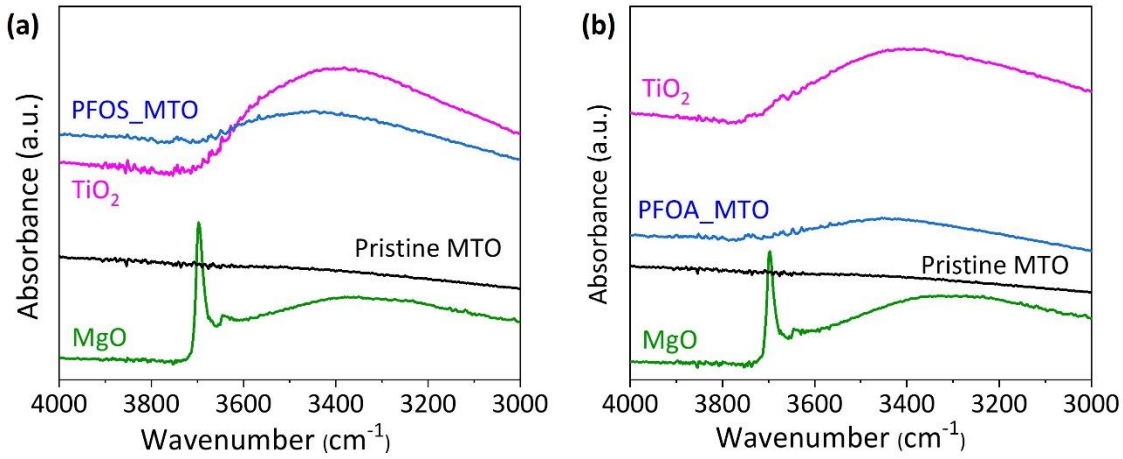

Figure S3. FTIR spectra of MgO, TiO_2, and MTO before and after (a) PFOS and (b) PFOA adsorption in the range of 4000–3000 cm^{-1}. A broad absorption band around 3200–3600 cm^{-1}, typically associated with O–H stretching vibrations, indicates the presence of surface hydroxyl groups.

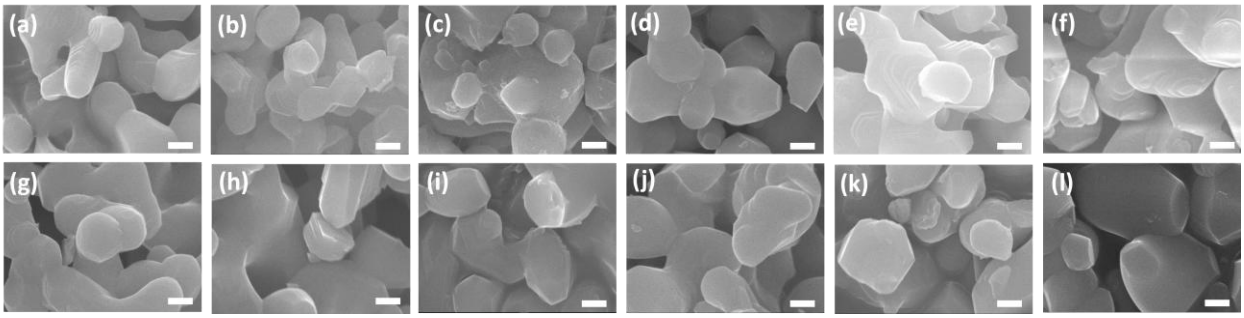

Figure S4. SEM images of MTO after PFOS (a–f) and PFOA (g–l) adsorption at pH 1.0–6.5. Scale bars: 300 nm.

References

1. W. J. Weber Jr and J. C. Morris, Kinetics of adsorption on carbon from solution, *J. Sanit. Eng. Div., ASCE*, 1963, **89**, 31-59.

2. Y. S. Ho and G. McKay, Pseudo-second order model for sorption processes, *Process Biochem.*, 1999, **34**, 451-465.

3. N. Chiron, R. Guilet and E. Deydier, Adsorption of Cu (II) and Pb (II) onto a grafted silica: isotherms and kinetic models, *Water Res.*, 2003, **37**, 3079-3086.

4. I. Langmuir, The adsorption of gases on plane surfaces of glass, mica and platinum, *J. Am. Chem. Soc.*, 1918, **40**, 1361-1403.

5. H. Freundlich, Über die adsorption in lösungen, *Z. Phys. Chem.*, 1907, **57**, 385-470.

6. R. Sips, On the structure of a catalyst surface, *J. Chem. Phys.*, 1948, **16**, 490-495.

7. G. P. Jeppu and T. P. Clement, A modified Langmuir-Freundlich isotherm model for simulating pH-dependent adsorption effects, *J. Contam. Hydrol.*, 2012, **129**, 46-53.

8. E. Steinle-Darling and M. Reinhard, Nanofiltration for trace organic contaminant removal: structure, solution, and membrane fouling effects on the rejection of perfluorochemicals, *Environ. Sci. Technol.*, 2008, **42**, 5292-5297.

9. D. Brooke, A. Footitt and T. Nwaogu, Environmental risk evaluation report: Perfluorooctanesulphonate (PFOS), *Environment Agency: Bristol, U.K.*, 2004. 1–104.